Construction and Building Materials 192 (2018) 538–554

Contents lists available at ScienceDirect

Construction and Building Materials

journal homepage: www.elsevier.com/locate/conbuildmat

Static response of asymmetrically damaged metallic strands: Experimental and numerical approach

Juan Felipe Beltrán [a,*], Eduardo Nuñez [b], Fernanda Nuñez [b], Ismael Silva [b], Tomás Bravo [b], Ricardo Moffat [c]

[a] Dept. of Civil Engineering, University of Chile, Blanco Encalada # 2002 Of. 440, Santiago, Chile
[b] Inst. Civil Engineering, Austral University, Valdivia, Chile
[c] Dept. of Civil Engineering, Adolfo Ibañez University, Diagonal Las Torres # 2640 2002, Santiago, Chile

HIGHLIGHTS

- Static strands response with asymmetric surface damage is studied.
- A nonlinear beam-based model is proposed to assess damaged strand response.
- Test data and 3D FE simulations validate the proposed nonlinear beam-based model.
- The nonlinear-based model is a robust and computationally cheap tool.

ARTICLE INFO

Article history:
Received 4 July 2018
Received in revised form 12 October 2018
Accepted 15 October 2018
Available online 25 October 2018

Keywords:
Asymmetric damaged strands
Surface damage
Numerical model
Finite element simulation
Experimental test
Static capacity curve

ABSTRACT

In this study, the effect of the presence of broken wires (damage) asymmetrically distributed on metallic strands surfaces on their static response is assessed. To this end, a general mechanical model for multi-layered strands is presented, in which damaged strands are treated as a 1D nonlinear beam under uncoupled biaxial bending and axial load (*NLBM*). The *NLBM* is validated by comparisons with the results obtained from an experimental program especially designed for studying the effect of surface damage distribution on strands response and 3D nonlinear finite element simulations. Analyses are carried out on two strand constructions: 1×7 and 1×19, in which the damage levels and strand diameters vary from 5% to 40% and from 3.5 mm to 22.2 mm, respectively. Results indicate that the *NLBM* accurate predicts the static response (residual strength, stiffness, axial strain field, and deformed configuration) of the asymmetrically damaged strands, achieving good computational efficiency and numerical robustness.

1. Introduction

A strand can be a critical structural member in many engineering applications, including cranes, lifts, mine hoisting, bridges, cableways, electrical conductors, offshore mooring systems and so on. Different classes of strands, suited for different purposes, have a different number and arrangement of strand components within the strand cross-section in which the components can be made of different materials. Over the years, each field of strand application has developed a specific body of knowledge, based on extensive testing and field experience, leading to empirical rules for each particular application. Unifying these empirical rules under some general mathematical and mechanical theory would allow a better understanding, and in the long term, a better prediction of the mechanical behavior of strands as well as reduce the need for expensive tests under a variety of operating conditions. Thus, due to their extensive use and the need to predict their behavior, several researchers have presented analytical models that permit the calculation of rope response based on the strand component material and geometry [1].

Strands made of filaments drawn from ductile metals are widely used as structural components. In particular, the extensive use of steel wire strands for load bearing components is mainly due to the strength offered by steel coupled with the flexibility of strand construction, strand geometry and wire size that can be suited to the required application. On the other hand, aluminium-based strands are widely used in transmission lines (conductors) due to their high conductivity to weight ratio leading to reduce the size of the support structures. In any of the applications previously mentioned, strands are subjected to various loading conditions. Although a strand is essentially an element for transmitting a tensile load, its construction is such that the individual wires in a strand are subjected to bending and torsional

* Corresponding author.
E-mail addresses: jbeltran@ing.uchile.cl (J.F. Beltrán), eduardo.nunez@uach.cl (E. Nuñez), fernanda.nunez@ing.uchile.cl (F. Nuñez), ismael.silva@ing.uchile.cl (I. Silva), tomas.bravo@ing.uchile.cl (T. Bravo), ricardo.moffat@uai.cl (R. Moffat).

https://doi.org/10.1016/j.conbuildmat.2018.10.092
0950-0618/

moments, frictional and bearing loads, as well as tension. The magnitude and distribution of the stresses resulting from these loadings determine the overall strand/conductor response, which can be expressed in terms of the extension and rotation of the strand/conductor [2]. In the following, the descriptions given are valid for both steel strands and aluminium conductors unless otherwise specified; hence, just strand is used hereafter to avoid repetitive use of the term strand/conductor.

Strands experience damage throughout their loading history and from continued aggression of the environment (urban, industrial, marine, heat exposure, chemical, etc). The process by which damage occurs can be represented through a degradation of the properties of individual strand wires, and it can also include the complete rupture of one or more wires. The understanding of the interaction of the factors that induce damage to strand and their dependence on strand operational conditions are essential to estimate strand service life at the design stage and to establish the appropriate strand inspection methods and discard criteria. Hence, the service life of a strand can be greatly extended by following a planned program of installation, operation, maintenance, and inspection. In this context, damage-tolerance property (i.e., the ability of a strand to withstand damage) is an essential parameter for strand design, strand evaluation during operational service, and for developing discard criteria according to strand usage based on the residual strength and deformation capacity that the damaged strand can sustain [3].

Symptoms of strand degradation, which are related to the most common discard criteria utilized to remove damaged strands after inspections, are the number of broken wires, reduction in strand diameter, excessive corrosion, and strand deformation (waviness, birdcage, loops, loose wires, nodes, and kinks among others) [4–6]. Experimental [7–11] and numerical [12–15] studies on metallic strands, mainly conducted on steel wire ropes, have intended to determinate the ability of particular types of strand constructions to withstand damage (i.e., damage-tolerance property). More precisely, considering a variety of wire breaks distribution, strands constructions, and loading conditions, aforementioned works have mainly focused on the determination of the residual strength [7,8,12] and axial strain field on strands cross-sections and along the length of the strands [9,10,13,14]. Others have monitored damage evolution to establish reliable conditions of damaged strands use [10,11,15]. The results of previous studies have shown that, in particular, the impact of broken strand components on overall strand response (stiffness, residual strength, deformation capacity, and deformed configuration) depends on the length of the strand, number of broken strand components (degree of damage or damage level), type of strand construction, and their distributions throughout the strand cross-section (symmetric and asymmetric) and along the strand length. For the purpose of this study, damage is referred to the presence of fully ruptured wires in the strand cross-section.

In this paper, the effect of a particular damage distribution on metallic (steel and aluminium) strand static response is assessed through experimental tests and numerical simulations. The damage is asymmetrically distributed on the outermost strand layer to simulate surface damage (degradation due to corrosion, abrasive wear, and fatigue among others). To this end, a general mechanical model for multilayered strands asymmetrically damaged on their surfaces is presented, in which damaged strands are treated as a 1D nonlinear beam under uncoupled biaxial bending and axial load (*NLBM*). This proposed model is an extension of the model presented in [16], originally developed for single-layer ropes, to account for multilayered strand geometry, which is validated by comparisons with experimental data and 3D nonlinear finite element simulations. Experimental data are obtained from tensile tests conducted on galvanized steel and aluminium strands asymmetrically damaged on their surfaces. The validation process of the *NLBM* accounts for two strand constructions: 1×7 and 1×19, whose diameter values range from 3.5 mm to 22.2 mm and the damage levels from 5% to 43% relative to the virgin cross-section, in which damage is artificially inflicted at strands midspan by cutting a prescribed number of wires. The analyses performed validate the extended model which is used to interpret and extend the experimental data reported in this study. As such, a robust and computational efficient numerical tool to assess damage-tolerance property of metallic strand asymmetrically damaged on their surfaces is presented. This tool may assist in quantifying the variations in performance of damaged strands that should be anticipated when predicting service life and in evaluating the coupling of some of the discard criteria parameters used in strands that are built into many standards such as the number of broken wires, waviness, and residual strength.

2. Experimental set up and materials

Steel (ST) and aluminium (AL) strands are tested in this work. Steel strands cross-sections consist of six wires helically wrapped around a straight central wire (core)(ie., $1 \times 7 = 1 + 6$ strand). On the other hand, two types of cross-sections are considered for the aluminum strands specimens: (1) 1×7 strands and (2) a single straight wire (core) followed by six and twelve helically wound wires in two concentric layers (i.e, $1 \times 19 = 1 + 6 + 12$ conductor). Geometrical parameters and minimum breaking strength (MBS) of the test specimens are listed in Table 1, in which the lay angle is the angle between the local longitudinal axis of the wire relative to the global longitudinal axis of the strand. The MBS values are provided by the strands suppliers as well as the lay direction of the wires at each layer, in which L.H and R.H stand for left and right hand respectively. The computed fill factor values of the strand specimens range from 0.75 to 0.78.

For the (1×7) and (1×19) specimens previously described, four types of tensile tests are performed: intact (virgin) specimen and three specimens asymmetrically damaged on their surfaces (outermost layer) at strands midspan. Damage to cross-section considers from one to three wires completely cut on specimens surface for the former case and from two to six wires for the latter case as depicted in Fig. 1, in which cut wires are colored black.

Damage level (percentage of loss of cross-sectional area) and degree of asymmetry in damage distribution (measured by the index of asymmetry explained later in Section 3) values are selected to have similar values used in a previous work [16]. As such, damage level and degree of asymmetry values range from 5% to 43% and from 0.167 to 0.5 respectively. In this way, a wide range of values of these two parameters are used to validate the proposed model presented in this study. Tensile tests are carried out using an Instron 600LX universal testing machine with a maximum tensile capacity of 300 kN. Strands axial strains are measured using LVDT and extensometers for the case of the intact specimens and LVDT for the case of damaged specimens (Fig. 2a). Based on experimental, analytical, and numerical studies [9,10,16], it is expected that asymmetric damage distribution induces a gradient in the axial strain distribution throughout strand cross-section, in which the axial strain values are maximum in the wires adjacent to damage and minimum in the opposite ones. In order to experimentally validate this assumption, strain gauges are used to measure the axial strain developed by adjacent and opposite wires to damage as shown in Fig. 2b, in which a 23.5 mm diameter coin is used as an attempt to show the size of the strain gauge. Resin socketing is used for terminating strand specimens in which the length between sockets is 600 mm accordance with the provisions in ISO 3108:2017. Tensile capacity tests are performed under displacement control at a rate of 5 mm/min.

Table 1
Geometrical properties and minimum breaking strength of the test specimens.

Strand	Strand Diameter [mm]	Material	Number of wires	Mínimum Breaking Strength (kN)	Wire Diameter [mm]	Layer	Lay angle [°]	Lay direction
1 × 7	9.5	ST	7	68.5	3.10	2	7.5	L.H
1 × 7	10.1	AL	7	19.7	3.37	2	8	R.H
1 × 7	12.7	ST	7	119.7	4.19	2	8	L.H
1 × 7	14.3	AL	7	37.8	4.77	2	7	R.H
1 × 19	19.9	AL	19	69.3	3.98	2	8.7	L.H
						3	11.7	R.H

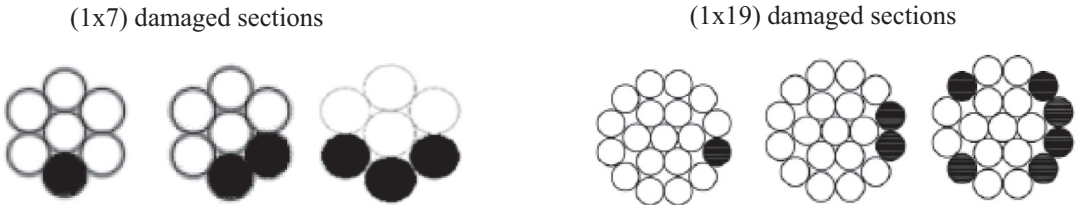

Fig. 1. Steel strands and aluminium conductors damaged cross-sections.

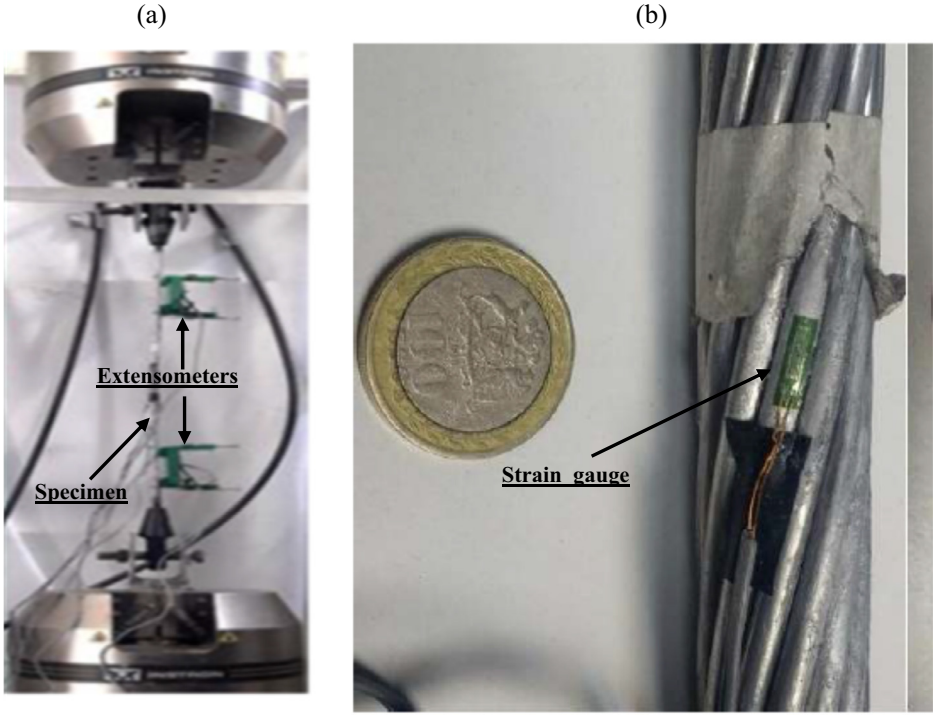

Fig. 2. Sensors to measure strains: (a) extensometers (b) strain gauge.

3. Numerical approach

In the particular case of ropes (metallic and synthetic fiber) asymmetrically damaged, some efforts have been made in order to numerically and analytically assess the impact of damage on their response [10,12,16–18]. This information could be later utilized to establish if the structural integrity of the damaged strands, and also the integrity of the structural system that they are part of, is compromised. In the current study, the model proposed by Beltran and De Vico [16], which is established for a single-helically layered strand, is extended to account for a multilayered strand geometry in which broken wires are asymmetrically distributed in the outermost layer to simulate surface damage.

3.1. Description of the simplified numerical model

In the extended proposed model, the asymmetrically damaged strand is assumed to behave as a nonlinear beam (*NLBM*) under biaxial bending and axial load with Bernoullís kinematic hypothesis (i.e, stick-state kinematic assumption). As explained in [16], biaxial bending arises from the unbalanced radial contact forces within a strand cross-section due to the asymmetric damage distri-

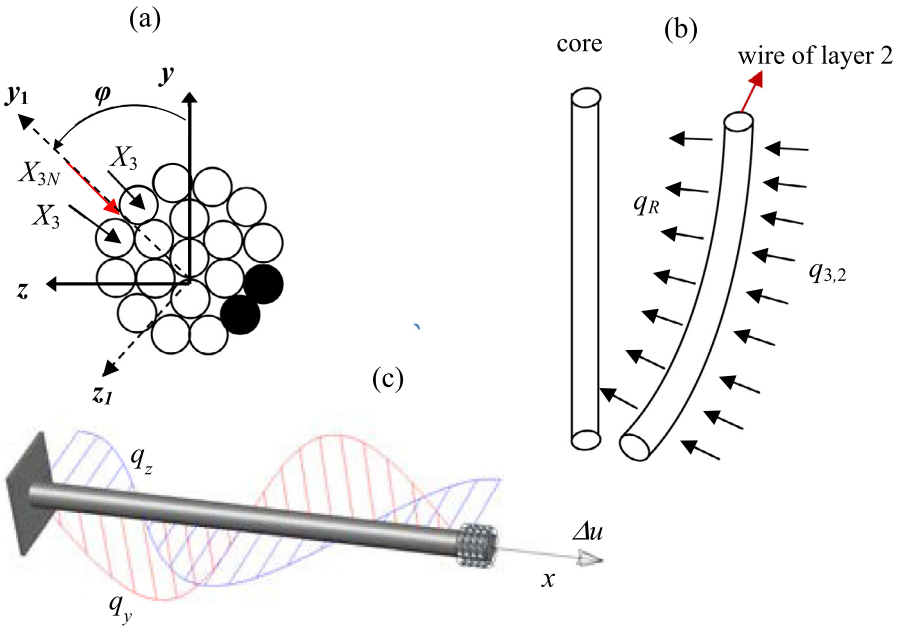

Fig. 3. (a) Asymmetrically damaged multilayered strand cross-section; (b) Interlayer contact pattern; (c) nonlinear beam under sinusoidal loads.

bution, resulting in a net transverse force per unit length of strand q_R, which is decomposed into the principal planes (xy and xz) of the damaged strand cross-section (Fig. 3a). The magnitude of the net transverse force q_R accounts for the initial helical geometry of the unbroken strand components.

According to the model proposed in [16], the static response of an asymmetrically damaged strand is governed by the following equations:

$$(EI_{zz})_{sec}\frac{d^4v}{dx^4} - q_y(x)\left(1+\frac{du(x)}{dx}\right) - H(x)\frac{d^2v}{dx^2} = 0 \quad (1)$$

$$(EI_{yy})_{sec}\frac{d^4w}{dx^4} - q_z(x)\left(1+\frac{du(x)}{dx}\right) - H(x)\frac{d^2w}{dx^2} = 0 \quad (2)$$

where the plane directions z and y coincide with the principal axes of the damaged cross-section; $q_y(x)$ and $q_z(x)$ are the distributed forces along the rope length in the y and z direction respectively; $(EI_{zz})_{sec}$ and $(EI_{yy})_{sec}$ are the secant bending stiffnesses of the strand component with respect to the z and y axes, respectively; $v(x)$ and $w(x)$ are the deflections in the xy and xz (principal) planes, respectively; $u(x)$ is the displacement of the centroid in the axial direction; and $H(x)$ is the horizontal force relative to the axial direction of the undeformed damaged strand.

The procedure implemented to compute the expressions for $q_y(x)$ and $q_z(x)$ is extended relative to the one described in [16] due to the increasing complexity of the damaged cross-section strand analyzed in the current study as previously stated. The determination of the net unbalanced line force q_R is based on the assumption that contact between wires is assumed to be only in the radial direction (the so-called interlayer contact forces). The process, and related assumptions, of estimating the value of q_R for the case of a multilayered strand, whose damaged cross-section for illustrative purposes is depicted in Fig. 3a, is outlined in the subsequent steps.

- Consider the asymmetrically damaged strand cross-section depicted in Fig. 3a. This is a three-layered strand in which in the terminology used in this study the core is always considered to be the first layer. Damage is inflicted in the third (outermost) layer in which cut wires are colored black.
- Assuming interlayer contact pattern between strand wires, helical wires that belong to the third layer are not in radial equilibrium due to the loss of symmetry of that layer associated to the asymmetry in damage distribution. The radial line body forces X_3 of the two wires opposite to damage are unbalanced resulting in net radial line force X_{3N} pointing to the centroid of the strand (Fig. 3a). For clarity purposes, only the radial line body forces X_3 of the wires opposite to damage are depicted, because the others cancel out in pairs. The value of the radial line body force X_3, considering each wire as a tensile element, can be estimated as $\kappa_3 T_3$ where κ_3 and T_3 is the curvature and tensile load of a helical wire located in layer 3, for a given value of the strand axial strain ε [19].
- The resulting unbalanced net radial line force X_{3N} is transmitted from the outer to inner layers, considering the distance between points of contact (discrete contact pattern) along a helical wire as described in [20]. In this particular example, the transferred value of X_{3N} to layer 2, $q_{3,2}$, is given by

$$q_{3,2} = \frac{p_2 cos\,\bar{\alpha}_2}{p_3 cos\,\underline{\alpha}_3} X_{3N} \quad (3a)$$

where the angles $\underline{\alpha}_3$ and $\bar{\alpha}_2$ are defined as $\tan^{-1}(p_3/2\pi(a_3-r_3))$ and $\tan^{-1}(p_2/2\pi(a_2-r_2))$, respectively, where p_i is the pitch distance, a_i is the helix radius and r_i is the radius of a wire in layer i, with $i = 2,3$ for this particular example (Fig. 3b).

- From layer 2, the effect of the unbalanced radial line force has to be transmitted to the core of the strand in order to analyze the damaged strand as a beam element subjected to axial and bending loadings (Eqs. (1) and (2)) do not include torsional terms). Accounting for the continuous radial contact between wires in

the second layer and the strand core, the value of the unbalanced radial line force q_R acting along the longitudinal axis of the strand is given by

$$q_R = \frac{1}{\cos\theta_2}\left[\frac{p_2 \cos\bar{\alpha}_2}{p_3 \cos\underline{\alpha}_3} X_{3N}\right] \tag{3b}$$

where θ_2 is the lay angle of the wires that belong to the second layer of the strand (Fig. 3b). In the general case, the unbalanced radial line force q_R acts in the $-y_1$ direction forming an angle φ relative to an arbitrary axis y, in which y_1 is the axis of symmetry (also a principal axis) of the damaged strand cross-section. Due to the helical nature of the wires, the principal plane z_1y_1 coincides with the arbitrary plane zy for increasing values of φ (Fig. 3a) equal to $n\pi/2$ (n is an integer). As proposed in [5], instead of rotating the principal plane z_1y_1 along the longitudinal axis of the damaged strand due to the helical nature of the wires in their initial configuration, the analysis of the damaged strand is approximated by considering the arbitrary plane zy as the principal one (that is valid when z_1y_1 and zy coincide) and varying the net transverse forces in both xy and and xz planes, $q_y(x)$ and $q_z(x)$, along the strand longitudinal axis x throughout the relationship $\varphi = (2\pi x/p_2)$ where p_2 is the pitch distance of the wires that belong to the second layer. As such, the damaged strand is analyzed with a constant cross-section and the helical nature of strand wires in their initial configuration is captured by the sinusoidal net transverse forces $q_y(x)$ and $q_z(x)$ that induce a lateral deflection of the strand in the $-y_1$ direction (Fig. 3c). In the latter, one end of the strand is fully clamped and at the other end a uniformly increasing axial displacement history is specified (Δu) and the cross-section is prevented from rotating (displacement control analysis). According to Fig. 3a, the expressions to compute $q_y(x)$ and $q_z(x)$, which are present in Eqs. (1) and (2), are given by

$$q_y = \frac{1}{\cos\theta_2}\left[\frac{p_2 \cos\bar{\alpha}_2}{p_3 \cos\underline{\alpha}_3} X_{3N}\right]\cos\varphi \tag{4a}$$

$$q_z = \frac{1}{\cos\theta_2}\left[\frac{p_2 \cos\bar{\alpha}_2}{p_3 \cos\underline{\alpha}_3} X_{3N}\right]\sin\varphi \tag{4b}$$

- For a general multilayered strand geometry, that is a strand comprised of N layers, the resulting unbalanced net radial line force X_{NN} due to the asymmetry in surface damage distribution is transferred to layer 2, $q_{N,2}$, by the following expression:

$$q_{N,2} = \frac{p_2 \cos\bar{\alpha}_2}{p_N \cos\underline{\alpha}_N}\left(\prod_{k=3}^{N-1}\frac{\cos\bar{\alpha}_k}{\cos\underline{\alpha}_k}\right) X_{NN} \tag{5a}$$

where the variables involved in the above equation were already defined after presenting Eq. (3a). Following the above procedure, the value of the unbalanced radial line force q_R acting along the longitudinal axis of the strand is given by

$$q_R = \frac{1}{\cos\theta_2}\left[\frac{p_2 \cos\bar{\alpha}_2}{p_N \cos\underline{\alpha}_N}\left(\prod_{k=3}^{N-1}\frac{\cos\bar{\alpha}_k}{\cos\underline{\alpha}_N}\right) X_{NN}\right] \tag{5b}$$

Thus, the values of the sinusoidal net transverse forces $q_y(x)$ and $q_z(x)$ are respectively as follows:

$$q_y = \frac{1}{\cos\theta_2}\left[\frac{p_2 \cos\bar{\alpha}_2}{p_N \cos\underline{\alpha}_N}\left(\prod_{k=3}^{N-1}\frac{\cos\bar{\alpha}_k}{\cos\underline{\alpha}_k}\right) X_{NN}\right]\cos(2\pi x/p_2) \tag{5c}$$

$$q_z = \frac{1}{\cos\theta_2}\left[\frac{p_2 \cos\bar{\alpha}_2}{p_N \cos\underline{\alpha}_N}\left(\prod_{k=3}^{N-1}\frac{\cos\bar{\alpha}_k}{\cos\bar{\alpha}_k}\right) X_{NN}\right]\sin(2\pi x/p_2) \tag{5d}$$

Once the values of q_y and q_z in Eqs. (1) and (2) are estimated, these equations are analytically solved (i.e., they have closed-form solutions) for a given value of strand axial strain ε to compute the displacement field of a generic point of each unbroken strand wire [16]. The displacement field of a particular generic point at section x can be described assuming a stick-state kinematic model and using the component displacements $u(x)$, $v(x)$ and $w(x)$ of the damaged strand centroid at same section as follows:

$$u_x(x) = u(x) - y\frac{dv(x)}{dx} + z\frac{dw(x)}{dx} \tag{6a}$$

$$u_y(x) = v(x) \tag{6b}$$

$$u_z(x) = w(x) \tag{6c}$$

where $u_x(x)$, $u_y(x)$, and $u_z(x)$ denote the displacements in the x, y, and z directions, respectively (Fig. 3a), of the generic point ((z,y) location at strand cross-section) under consideration; and $d(\cdot)/dx$ is used for the first derivate.

A cross-sectional incremental-iterative numerical algorithm is implemented to estimate the static response of asymmetrically damaged strand, in which material and geometric nonlinearities are accounted for [16]. For completeness, a summary of the steps of this numerical algorithm for the jth incremental step of the analysis is provided in Appendix A.

3.2. Validation of the simplified model based on 3D FE simulations

The proposed numerical model is validated based on comparisons with the results extracted from traditional and well accepted 3D nonlinear FE approach. This numerical technique has been widely used to estimate the response of virgin and damaged cables under variety of loading conditions [17,21–24]. To this end, 3.5 mm and 22.2 mm diameter three-layered 1x19 steel strands are considered for validation purposes, which are commercially available and commonly used in antenna mast guys and suspension bridges. These two steel strands are not considered in the experimental program previously described and their numerical modeling is only for validation purposes. The computed fill factor values of the 1×19 steel strands is 0.77 and their geometrical properties and minimum and predicted virgin strength values are given in Table 2.

Table 2
Geometrical properties and strength values of (1x19) steel strands.

Strand diameter [mm]	Wires radius [mm]	Lay length (layer 2) [mm] (left hand lay)	Lay length (layer 3) [mm] (right hand lay)	Minimum Breaking Strength [kN]	Breaking Strength 3D FEM [kN]	Breaking Strength *NLBM* [kN]
3.5	0.35	28.6	42.5	9.7	9.72	9.81
22.2	2.22	181.5	270	354.5	389.3	398

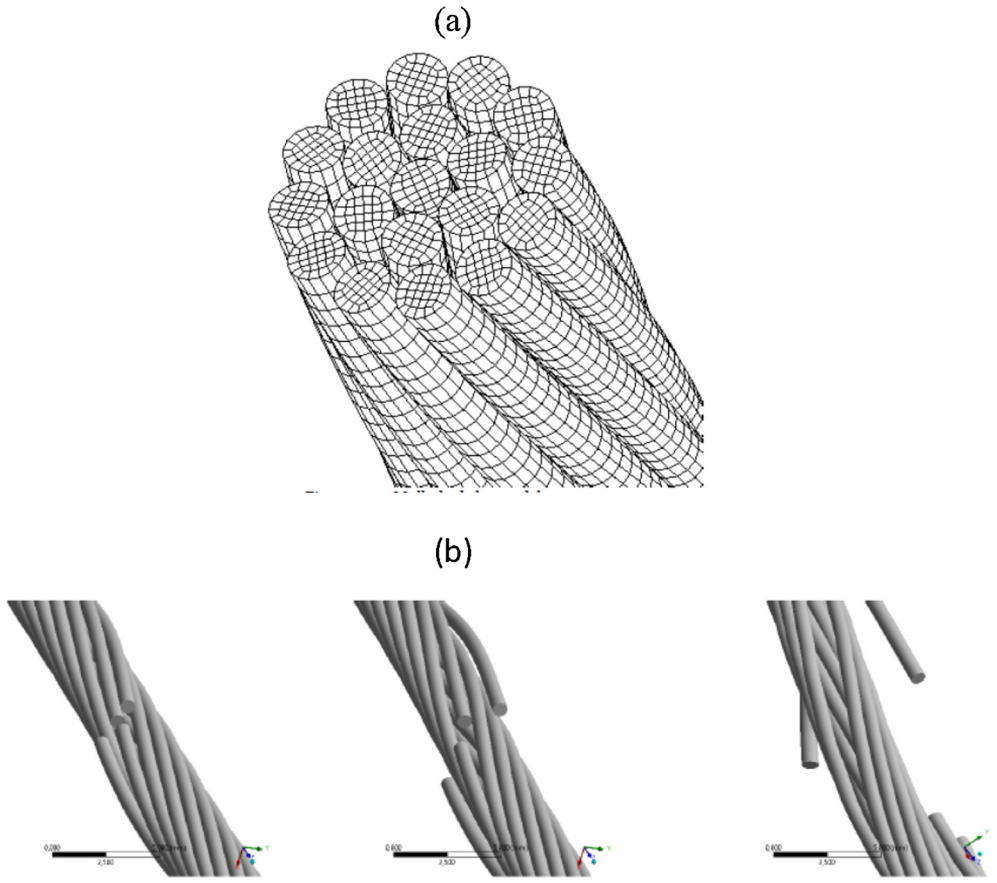

Fig. 4. (a) 3D FE mesh of a strand; (b) longitudinal view of a 3D FE damaged strand model for different values of axial strain.

For 3D FE modeling purposes the commercial software ANSYS is used having the steel strands the same geometry discretization. Each wire is discretized using Solid186 (ANSYS) three-dimensional linear finite elements that have three degrees of freedom at each node namely the translation in the x, *y* and *z* local directions. This element is selected due to its capabilities of supporting geometric and material nonlinear analysis and because it has been successfully used in modeling 3D synthetic-fiber and steel strands response [16,17,21]. A total of 33 linear brick elements (8-nodes elements) are used to discretize each wire cross-section in which its perimeter was divided into 16 brick elements, and the aspect ratio value of each element is set equal to 2:1 (length: width) in order to define its length. As such, considering the geometrical parameters given in Table 2, each wire is discretized into 304 intervals along its length which considers two pitch distances of the outermost layer of the strand length (Fig. 4a). For the case of the asymmetrically damaged strand 3D FE simulations, damage is deliberately inflicted at strands midspan location and simulated by inducing a discontinuity in selected strand wires. The discontinuity in the wires is achieved by doubling the nodes at particular locations (strands midpans in this case) without imposing compatibility conditions among them [17] (Fig. 4b). A wide range of friction coefficient values are examined (values range from 0.12 to 0.5) based on the information reported in the literature [14,25,26]. 3D FE numerical simulations show that the value of the friction coefficient has a minor impact on the monotonic axial response of a virgin and asymmetrically damaged strand [27].

Tensile capacity tests are conducted in order to obtain the constitutive law of the steel strand and aluminium conductor (later used in Section 4) wires. These tests are carried out on wires (W is used for wires in the corresponding plots) extracted from steel strands with diameters equal to 9.5 mm and 12.7 mm and from aluminum conductors with diameters equal to 14.3 mm and 25.3 mm. In both cases, an averaged engineering constitutive law is fitted based on ASTM E8 standard as depicted in Fig. 5. Average values of the mechanical properties of both materials are used for modeling purposes, considering a bilinear engineering constitutive law. For the steel (ST) case, these values are the following: Elastic modulus (E_{ST}) = 197,000 MPa; yield strain (ε_{yST}) = 0.0053; strain hardening modulus ($E_{sh\text{-}ST}$) = 5300 MPa; breaking strain (ε_{bST}) = 0.082. For the aluminium (AL) case, Elastic modulus (E_{AL}) = 65,000 MPa; yield strain (ε_{yAL}) = 0.0045; strain hardening modulus ($E_{sh\text{-}AL}$) = 525 MPa; breaking strain (ε_{bAL}) = 0.075. For the 3D nonlinear FE numerical simulations, the true stress–strain curve is provided as an input to the software (ANSYS), considering the following relationships: $\varepsilon_T = \ln(1+\varepsilon)$ and $\sigma_T = \sigma(1+\varepsilon)$, where ($\sigma$, ε) are the engineering values and (σ_T ,ε_T) are the true values of the normal stress and axial strain respectively.

In order to validate the proposed model (*NLBM*), comparisons of capacity curves and axial strain fields throughout strand cross-sections considering virgin and damaged three-layered steel strands with diameters equal to 3.5 mm and 22.2 mm are performed. These capacity curves are obtained from 3D FE simulations and from the *NLBM* in which the damaged ones consider two and six wires cut at strands midspan asymmetrically distributed on

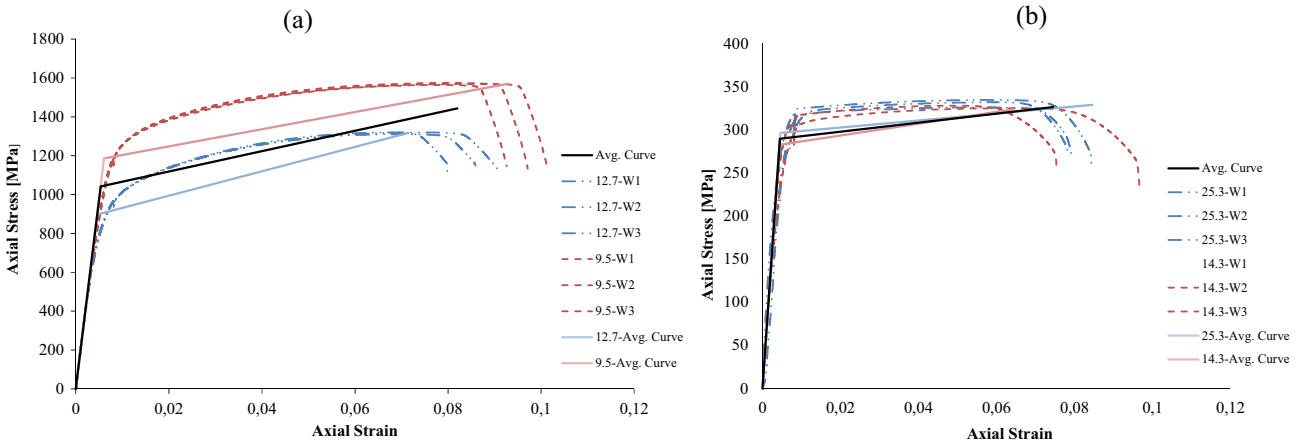

Fig. 5. Constitutive law for (a) steel and (b) aluminium.

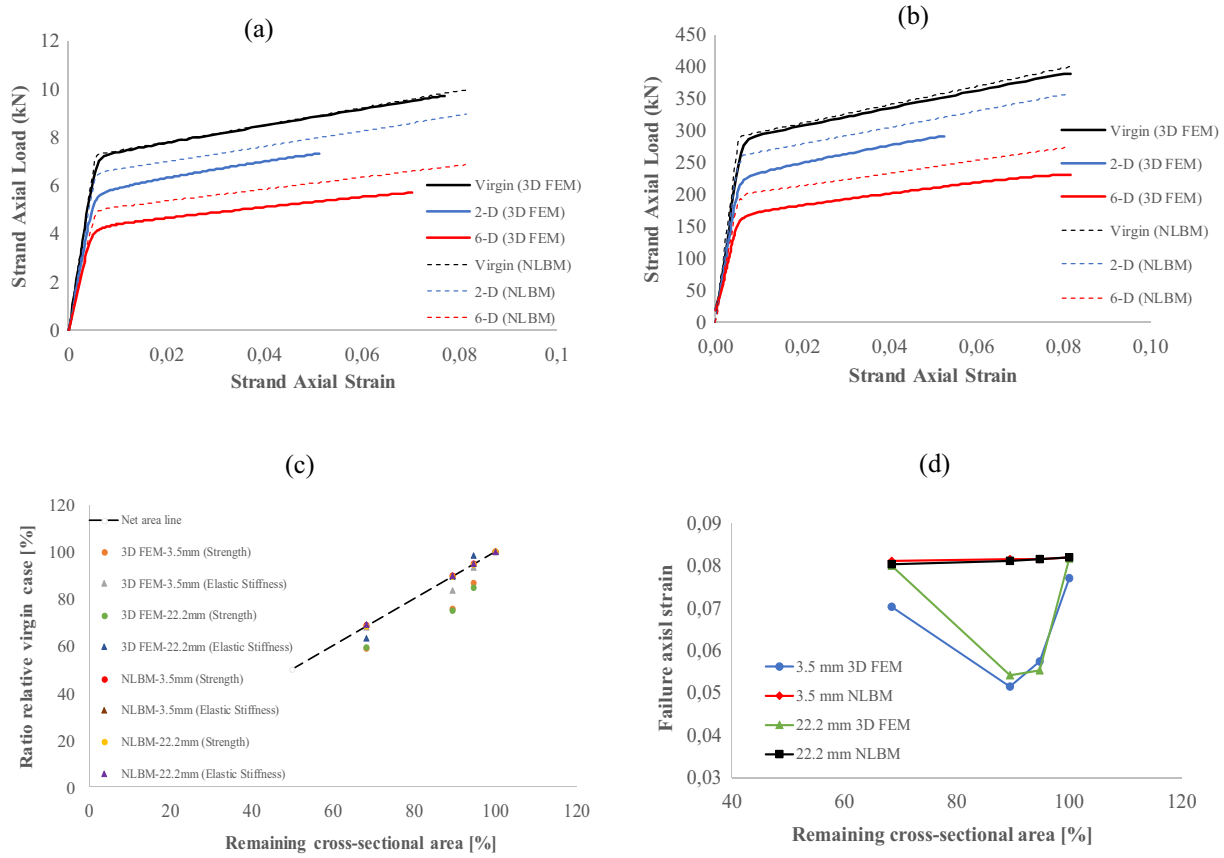

Fig. 6. Estimated capacity curves for (a) 3.5 mm and (b) 22.2 mm diameter steel strands with different damage levels; (c) reduction of residual strength and linear-elastic stiffness; (d) variation of the failure axial strain.

their surfaces. The Poissoń s ratio and friction coefficient values considered for performing 3D FE simulations are equal to 0.3 and 0.115, respectively [24].

As shown in Fig. 6a and b, virgin capacity curves, considering engineering strain values, compare quite well between each other for both strand sizes, in which the minimum breaking strength (by strand manufacturer) and estimated by both *NLBM* and 3D FEM are listed in Table 2. For the case of damaged curves, for analysis purposes, it is considered one (1-D), two (2-D), and six (6-D) out of nineteen wires cut (Fig. 1) corresponding approximately from 5% to 32% of the strand cross-section damaged. Due to the complex interaction between undamaged wires, the yield load predicted by 3D FE simulations are lower than the ones predicted by *NLBM* that ignore all the contact patterns between strand wires. *NLBM* overestimates the yield load and residual strength (maximum capacity) values relative to the 3D FE ones in about 20% and 15% respectively, inducing a larger linear response of the damaged strands. However, the linear and post-yielding stiffnesses provided by both models compares quite well between each other. Specifically, in Fig. 6c, the non-dimensional parameters related to residual

strength and linear-elastic stiffness provided by both model are compared between each other and relative to the net area line (model). Both non-dimensional parameters are the ratios of the corresponding damaged variables relative to their undamaged (virgin) values for each of the models presented; and the net area line accounts for the fact that the reduction in strand strength and strand linear-elastic stiffness is proportional to the damage level inflicted on the strand. Based on the results presented, *NLBM* estimates a reduction in both parameters proportional to the level of damage inflicted (i.e, results lie on the net area line). For the case of the 3D FEM results, predicted linear-elastic stiffness values somewhat deviate from the net area line (maximum underestimation relative to this line model is 7%) and for the case of the residual strength, deviation from this line ranges from −8% to −15%, in which the maximum deviation is reached for the case of two wires (2-D) cut.

Estimated capacity curves previously presented are plotted up to the failure of the first initial unbroken wire predicted by the corresponding numerical models (3D FEM and *NLBM*) based on the maximum failure strain criteria (failure true strain value equal to 0.079). In this way, the capacity curves of damaged strands for particular damage distributions are assessed, not considering the following continuous change in damage distribution due to the progressive failure of the strand cross-sections. Based on 3D FEM results, strands with one and two wires initially cut present premature wire failure relative to the strand with initially six wires cut (Fig. 6d). The presence of isolated damage (one or two wires cut; Fig. 1) seems to amplify the effects of singularities in the model (normal and tangential shear contact stresses in the contact regions between wires) inducing higher axial strain and resulting in a premature failure of the most strained wires (values between 50% and 60% of the virgin case). The latter is supported by the analysis of the strain field developed throughout damaged strand cross-sections presented in the subsequent paragraph and Fig. 7. Contrary, a more distributed damage (six wires initially cut) seems to perturb less the damaged strand geometry, contact forces are better distributed not inducing premature failure in the most strained wires. More details on this issue can be found in [27]. In fact, similar failure axial strain values to the virgin ones are predicted by 3D FEM for the six wires damaged strand (Fig. 6d) as estimated by the *NLBM*, which neglects the contact interaction between wires in the calculation of the strain field. Thus, the latter model predicts a slightly reduction in the failure axial strain values relative to the virgin case as the damage level increases (Fig. 6d).

Regarding the axial strain field throughout damaged strand cross-section predicted by both numerical models (*NLBM* and 3D FEM), two levels of true axial strand deformation are chosen for comparison purposes (Fig. 7), in which broken wires are colored black: 0.4% and 4%, values that correspond to the linear and

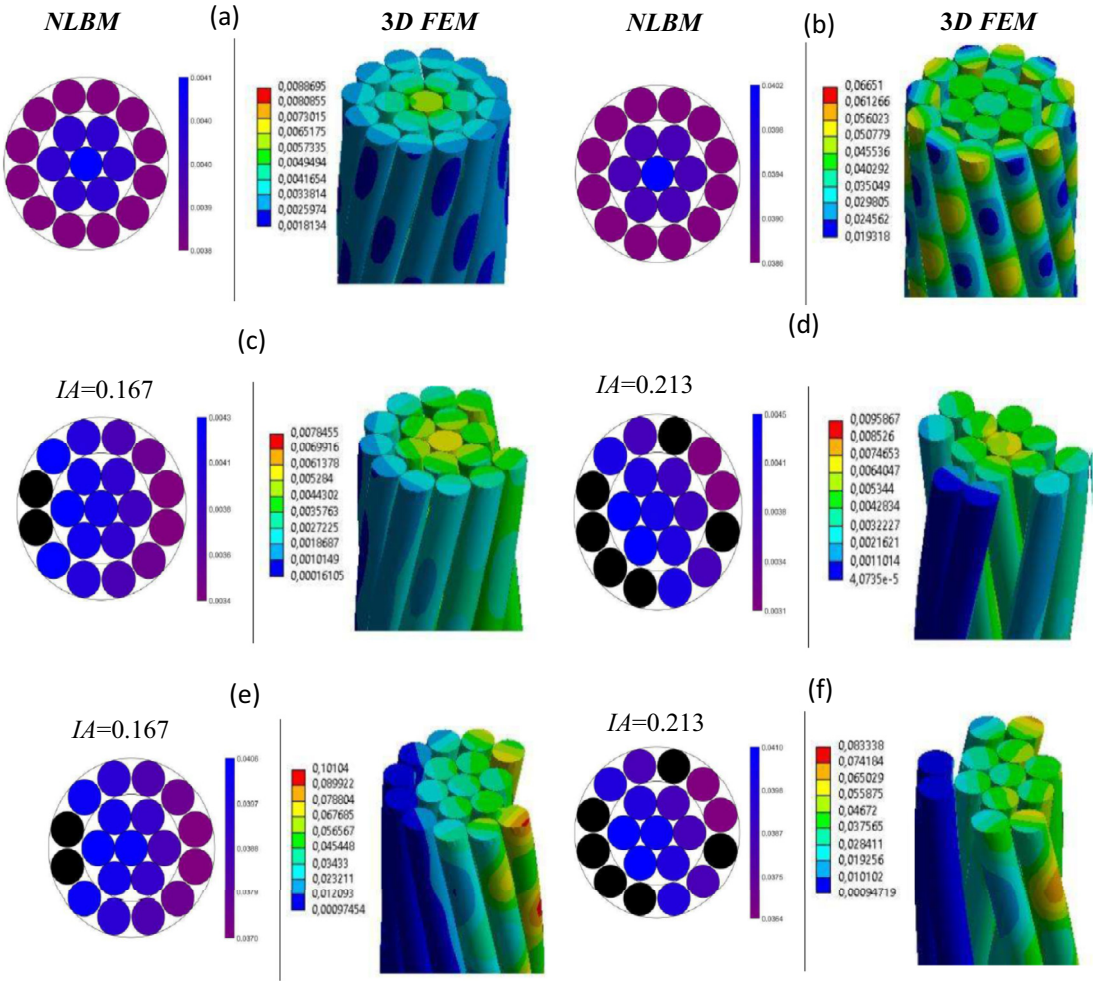

Fig. 7. Axial strain field for a 3.5 mm diameter strand at 0.4% axial deformation: (a) virgin case, (c) two wires cut, (d) six wires cut; 22.2 mm diameter strand at 4% axial deformation: (b) virgin case, (e) two wires cut, (f) six wires cut.

post-yielding (plastic) regime of damaged strand behavior respectively. It is important to point out that, after extensive analysis presented in [27], 3D FEM results suggest that axial strain distribution within damaged cross-section is constant along the strand's length, considering sections away from the strand ends. As such, the *NLBM*, which is a numerical algorithm that relies on a cross-sectional analysis, can be performed to estimate damaged strand response. In each figure, the left plot corresponds to the *NLBM* and the right plot to the 3D FEM. As a reference, strain distributions for the virgin case in also plotted in the aforementioned figure: Fig. 7a corresponds to the axial strain field through the virgin 3.5 mm diameter steel strand cross-section for an axial strain equal to 0.4% and Fig. 7b to the axial strain field through the virgin 22.2 mm diameter steel strand cross-section for an axial strain equal to 4%. In both cases, good agreement is obtained between the results provided by both models. For the damaged cases, as a general conclusion, neglecting local effects presented in the 3D FE simulations that amplify the effects of singularities in axial strain values, both numerical models predict similar maximum strain values developed adjacent to damage and a similar negative gradient in axial strain distribution in which strain values decrease for wires away to damage. Both strain distributions compare quite well between each other up to the inner surface of the undamaged wires opposite to damage (outermost layer of the strands). In these opposite wires, minimum axial strain values are developed, but 3D FE simulations are very sensitive to singularities and local effects that induce rapid changes in strain values throughout cross-sections of them which leads to estimate axial strain gradient equal to 100% for all the cases studied. This conclusion is valid for both elastic regime (Fig. 7c and d for a 3.5 mm diameter strand) and plastic regime (Fig. 7e and f for a 22.2 mm diameter strand). In the latter, comparing the results provided by the 3D FE simulations, the two wires cut configuration induces greater axial strain in the wires adjacent to damage (in the range of 0.06–0.1) than the six wires cut configuration (in the range of 0.04–0.075), which results in a premature failure of the wire in the former case as commented in Fig. 6a,b and d. Induced bending effect on axial strain values decreases for the six wires cut strand due the shifting of the neutral axis reducing the lever arm value of the most strained unbroken wires relative to the case of two wires cut strand.

Beltran and Vargas [17] proposed a scalar quantity termed the index of asymmetry (*IA*) to quantify the degree of asymmetry of the cross-section for particular damage level and damage distribution. This index captures the shift of the center of stiffness of the strand cross-section from its centroid due to the asymmetry of damage distribution as explained in detail in [17]. Based on the results shown in Fig. 7, as the index of asymmetry (values written above the damaged cross-sections) increases, the gradient in the axial strain field throughout strand cross-section, induced by the asymmetry in damage distribution, increases as well. Both models predict that maximum and minimum axial strain values are developed adjacent and opposite to damage, respectively. In particular, for the case of the 3.5 mm diameter steel strand with two (Fig. 7c) and six (Fig. 7d) wires cut considering a strand axial strain value equal to 0.4% (elastic regime), both models estimate that maximum and minimum axial strain values are 13% greater and 11% smaller than the virgin case (Fig. 7a) respectively, for the strand with two wires cut and 19% greater and 22% smaller for the strand with six wires cut. For the case of the 22.2 mm diameter steel strand considering the same damage distributions as in the previous case and a strand axial strain value equal to 4% (plastic regime), the maximum and minimum axial strain values are 5% greater and 4% smaller than the virgin case (Fig. 7b) respectively, for the strand with two wires cut (Fig. 7e) and 6% greater and smaller for the strand with six wires cut (Fig. 7f).

In order to further develop the analysis presented in Fig. 7, dependence on the *IA* values of the amplification factor, defined as the ratio between the maximum/minimum strain developed by a particular wire in a damaged state (considering one, two, and six wires cut) and the strain developed by the same wire in the virgin state, is shown in Fig. 8 based upon the results provided by the *NLBM*. In the latter, strand diameter and strand axial strain value (written in parenthesis) are indicated in the legends of the plots. For the case of the amplification factor associated to the maximum strain, f_{max}, (developed by wires adjacent to damage), in addition to increase as the *IA* value increases, these values are greater for the 22.2 mm diameter strand, suggesting that there is a diameter effect on the strain gradient developed in an asymmetrically damaged strand cross-section. Focusing on the elastic range, the amplification factor increases in 8% for the 22.2 mm diameter strand relative to the 3.5 mm diameter strand (Fig. 8a). The amplification factor associated to the minimum strain, f_{min}, (developed by wires opposite to damage) decreases as the strand diameter and *IA* value increase (Fig. 8b). In the elastic regime, this factor reaches a minimum value equal to 0.6 for the 22.2 mm diameter strand, 30% less than for the 3.5 mm diameter strand (diameter effect). Although the analysis conducted is mainly focused on the elastic damaged strands response, due to the safety factors used in their design [5] (values vary from 3 to 10 relative to the breaking load) that based upon the capacity curves shown in Fig. 6a and b, strands behave linear-elastic under their operational service, it is important to point out that in the plastic regime (plotted results for strand strain greater than 0.004 in Fig. 8), these amplification factors (both for the maximum and minimum wire strains) tend to approach 1 because net transverse forces magnitudes, $q_y(x)$ and $q_z(x)$ (Eqs. (4a) and (4b)), decrease due to the small value of the hardening modulus of the material (Fig. 5a). As such, the induced bending due to asymmetric damage distribution possesses lower influence on asymmetrically damaged strand response.

Based on the formulation of the *NLBM* and the results presented in Figs. 7 and 8, along with the gradient in axial strain field throughout strand cross-section (associated to the development of bending stresses), asymmetry in damage distribution also induces a lateral deflection in the damaged strand (Fig. 9a). This type of damaged strand behavior has been previously reported based on the results obtained from experimental studies [9,28,29]. In Fig. 9b and c, the maximum radial displacement estimated by both 3D FEM and *NLBM* for steel strands with diameters equal to 3.5 mm and 22.2 mm with one (1-D), two (2-D) and six (6-D) wires cut in their linear regime response are presented, respectively. The results presented by both numerical models compare quite well between each other in which the values predicted by the *NLBM* are in the range of [−15%, +12%] relative to the ones predicted by the 3D FEM (Fig. 9b and c). According to the ISO 4309 [6], one of the discard criteria for a damaged strand is the waviness (deformation) induced by an uneven stress distribution in strand cross-section that is this particular study is related to the asymmetric surface damage distribution (Fig. 9a). This induced waviness can accelerate wear damage in the outer wires of a

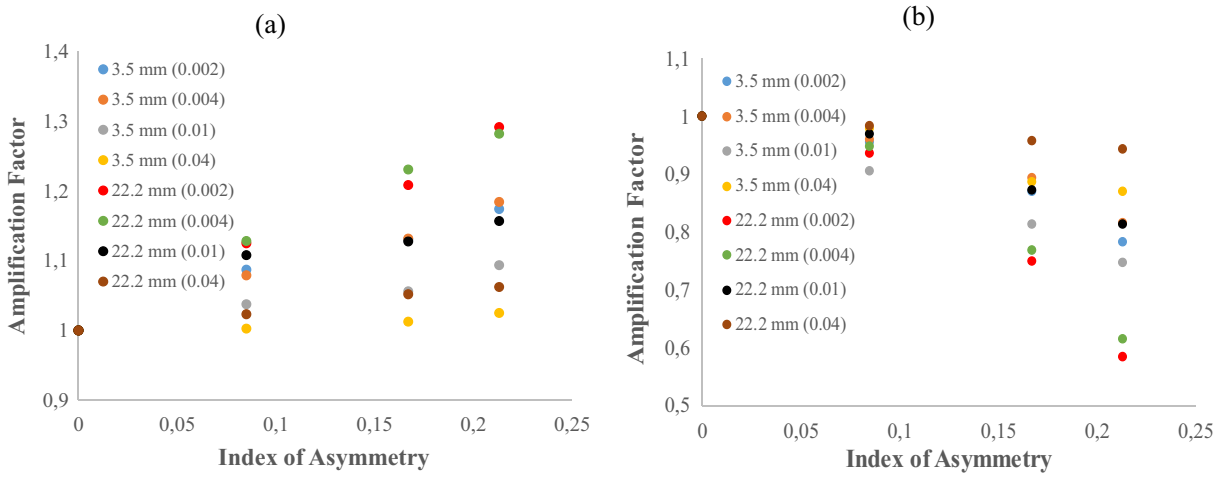

Fig. 8. Dependency of amplification factors on *IA* values predicted by the *NLBM*: (a) maximum strain; (b) minimum strain.

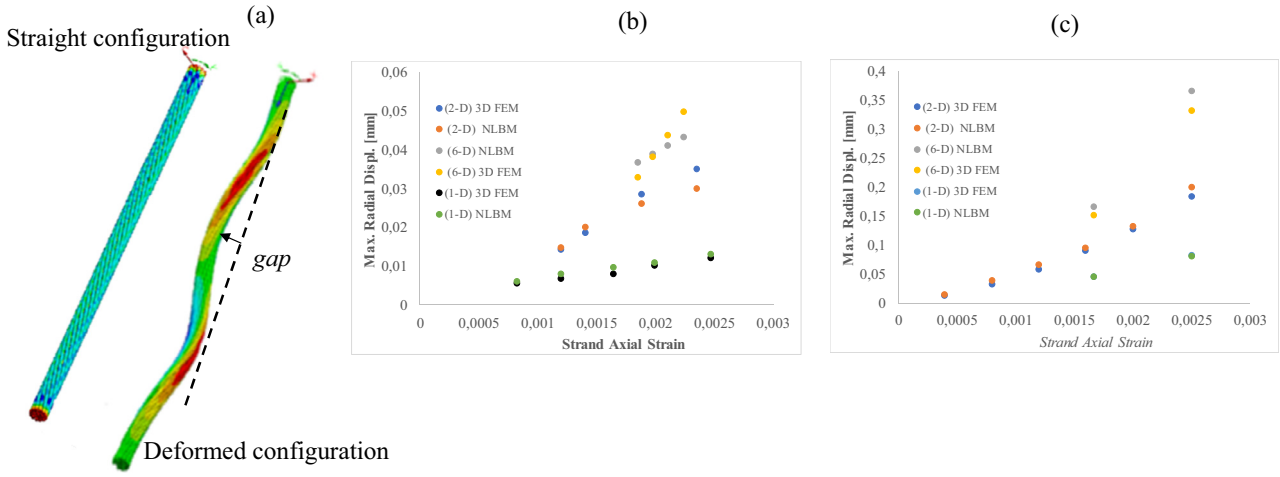

Fig. 9. (a) Sketch of the initial and deformed configuration of asymmetrically damaged strand; (b) and (c) maximum radial displacement for a 3.5 mm and 22.2 mm diameter asymmetrically damaged strands respectively.

strand. In hoisting strands, for example, waviness results in accelerated asymmetrical wear and plastic deformation as the strand passes over the sheave wheel and winding drum. The flattering of the outer wires will not be uniform around the strand circumference and broken wires can develop at this site with rapid deterioration in strand strength [30]. The waviness criteria establishes that the *gap* between a straightedge and the underside of the helix (Fig. 9a) should not be greater than 1/3*d* or 1/10*d*, being d the diameter of the strand, if the strand never runs through a sheave or spools on to the drum or if it does respectively. The *gap* can be safely estimated as twice the value of the maximum radial displacement experienced by the damaged strand. As such, for the entire range of damage level considered, the *gap* estimated for both strands are lower than the two aforementioned critical values. In fact, for the 3.5 mm and 22.2 diameter strands, the maximum radial displacement values are 1.4% and 1.7% of their diameter values respectively, considering in both cases six wires cut (6-D) (Fig. 9b and c).

It is worth to mention that the computational efficiency of the proposed model is very high relative to the results provided by the 3D FE nonlinear simulations. Few iterations (less than five) are needed to meet the set convergence criteria in *Step 8* of the proposed algorithm (Appendix A). For every capacity curve, strain field distribution and deformed configuration estimated by the *NLBM*, less than three minutes are needed to complete the computations on a standard multi-core processor laptop (Intel Core i7-16 Gb RAM). Conversely, 3D FE models are run on an Intel Xeon server 10 cores 2.2 GHz processor, 64 Gb RAM taking between 6 and 24 h to complete each analysis. The robustness of the *NLBM* is confirmed with the fact that all the capacity curves, strain distributions and deformed configurations associated to the damaged strands analyzed, compare well with 3D FEM results for two types of strand construction (1×7 and 1×19) accounting for a wide range of damage level and damage distribution (*IA* values).

4. Discussion of experimental results

In this section, the main results drawn from the experimental program conducted on asymmetrically damaged steel strands and aluminium conductors (hereafter referred as strands) are presented. In addition, the proposed model (*NLBM*) is used to extend

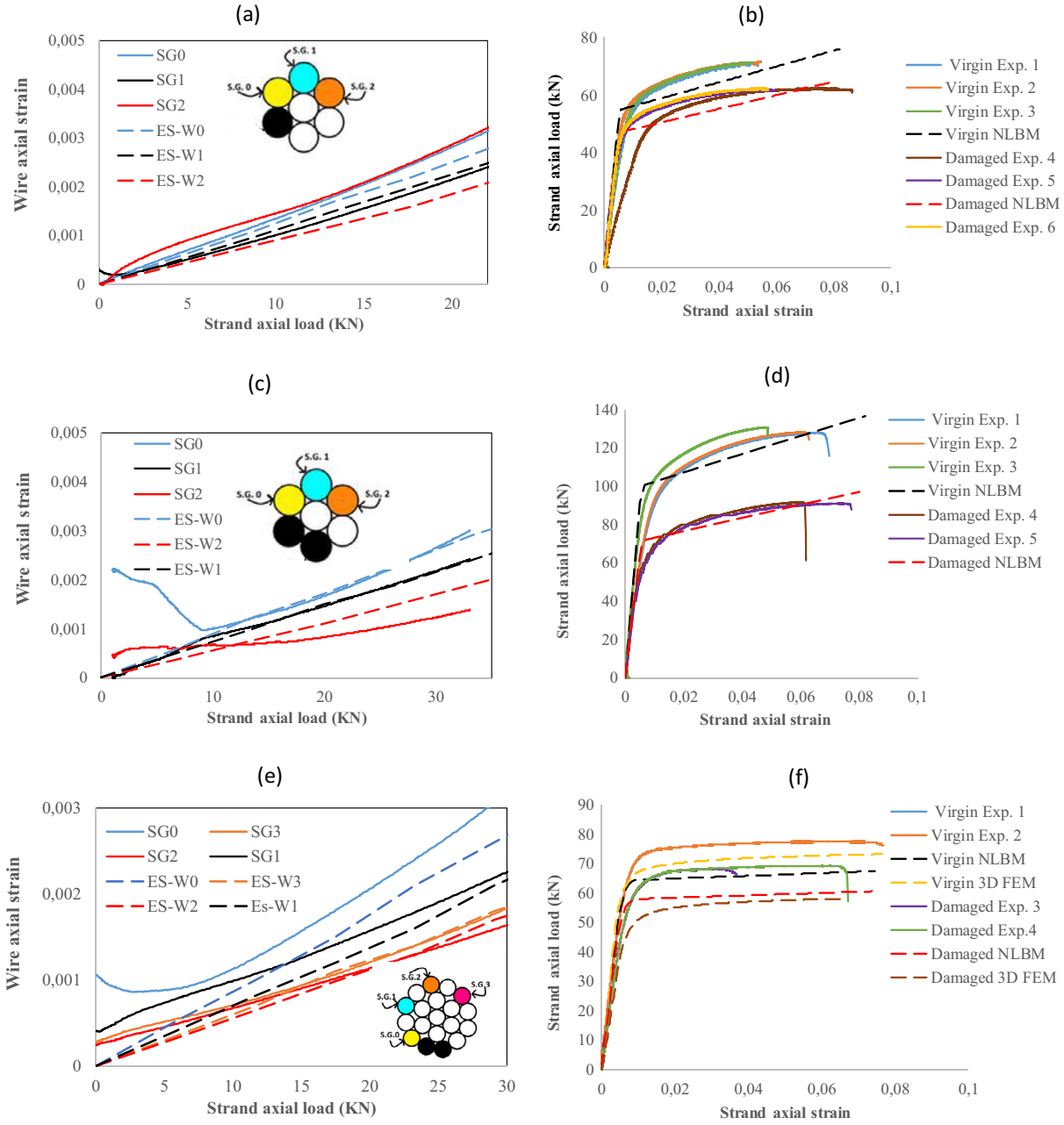

Fig. 10. Axial strain distribution on damaged strands cross-section and capacity curves: measured and predicted (*NLBM*) values.

and interpret the aforementioned experimental data along with performing an additional validation process of it.

Comparisons of the measured and predicted (by *NLBM*) capacity curves and axial strain distributions in the unbroken wires for some of the most representative specimens tested are presented in Fig. 10. As previously established in the Sub-Section 3.2, the analysis of the axial strain distributions in the unbroken wires is restricted to the elastic behavior of the strands and conductors considering the safety factors used in their designs [5] and the capacity curves shown in this figure. For the case of axial strain distribution, the nomenclature used to describe the results presented in this figure is as follows: SG_i is the strain measured with the *i*-th strain gauge placed on the surface of a particular wire sketched in the figure; $ES\text{-}W_i$ is the estimated strain provided by the *NLBM* developed in the wire over which the *i*-th strain gauge was placed. The position of the strain gauges within the damaged cross-sections and the damage distribution (cut wires are colored black) are depicted in the same figure. In general, good correlations are obtained between the measured and predicted axial strain values for all the cases shown in Fig. 10. Some local nonlinear response of the measured strain values, especially for low strand axial load values that induces deviations from the predicted ones, can be attributed to the initial bedding down process of the unbroken wires within the strands. In some particular cases (SG2 in Fig. 10c and SG0 in Fig. 10e), this initial nonlinearity strongly affects subsequent strain gauges measurements causing constant deviation between measured and predicted strain values relative to the other cases. Despite these particular cases, both measured and predicted values suggest that a gradient in axial strain distribution is developed in which greater strains take place adjacent

to damage and smaller strains opposite to damage (Fig. 10a,c and e). The latter agrees with the finding drawn in Sub-Section 3.2 as discussed in comments related to Fig. 7. The measured gradient, however, is greater than the estimated one: the ratio values between the maximum and minimum strain are in the range [1.8, 2.2] for the measured values case and in the range [1.32, 1.6] for the estimated values case.

Regarding the capacity curves presented in Fig. 10, both experimental virgin and damaged strands strength values are well estimated by the *NLBM*, in which these values are estimated within a range of −10% to +6%. The estimated initial virgin strand stiffness (i.e., linear elastic range) values given by the *NLBM* have good correlation with the experimental ones, in which the latter are predicted within a range of −10% to +4%. For the case of damaged strands, this estimate range increases approximately from −5% to 14% considering all the cases presented in Fig. 10. It is important to point out, that the reduction in the initial stiffness value due to damage given by the *NLBM* is proportional to the loss of cross-sectional area (i.e., net area effect) as discussed in detail later in Fig. 11. For the particular case of the 19.9 mm diameter aluminium strand (Fig. 10f), both virgin and damaged simulations based upon 3D FE models have been considered to strength the validation process of the *NLBM*, using Poisson's ratio and friction coefficient values equal to 0.33 and 0.5, respectively [25]. In both cases, there is a good correlation in terms of the estimates of the initial stiffness values. For the virgin strand response, the transition region from elastic to fully plastic behavior is wider for the case of the 3D FE model inducing a strength capacity conductor 8% greater than the one predicted by the *NLBM*. For the damaged case, 3D FE simulation

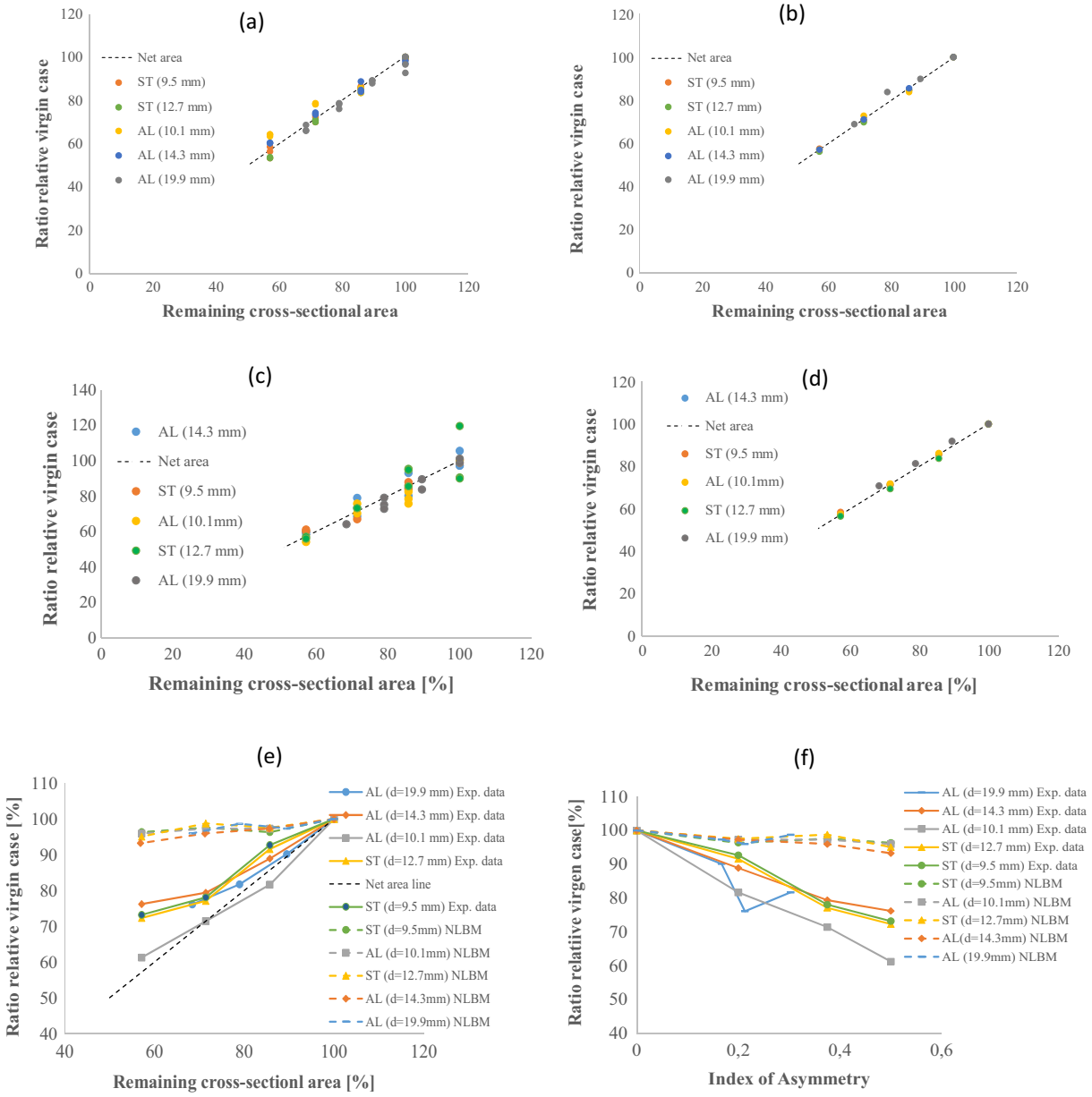

Fig. 11. Dependency of normalized values on remaining cross-sectional area: (a), (b) measured and estimated residual strength respectively; (c), (d) measured and estimated linear-elastic stiffness respectively; (e) measured and estimated deformation capacity. Dependency of normalized values on *IA* values: (f) measured and estimated deformation capacity.

gives an earlier transition from the elastic to the inelastic regime than the estimated by the *NLBM*, but considering that this transition region is wider for the former, *NLBM* overestimates the residual conductor strength in less than 4%.

In terms of the residual strength and initial elastic stiffness of the damaged steel and aluminium strands tested in this research project, the dependency of both parameters (normalized with respect to the virgin values) relative to remaining cross-sectional area is shown in Fig. 11. In general, for both parameters, experimental and estimated results lie on the net area line (dashed line). The net area line represents the fact that the reduction in strand strength and initial elastic stiffness is proportional to the loss of cross-sectional area due to damage. For the case of the residual strength parameter (Fig. 11a and b for measured and estimated values respectively), some deviation from the net are line is observed for measured values associated to the minimum value of the cross-sectional area considered in this study, which is equal to 57%. This deviation is consistent only for the 10. 1 mm diameter aluminium strand in which the measured residual strength is about 10% greater than the loss of cross-sectional area (Fig. 11a). This conclusion is consistent with earlier analysis reported in [16] on two layer small-scale (ropes diameter equal to 6 mm) asymmetrically damaged polyester ropes. In the latter, for values of the remaining cross-sectional area greater than 65%, estimated residual strength values provided by 3D FE and *NLBM* simulations slightly deviate from their corresponding net area curves. For the case of the initial elastic stiffness (Fig. 11c and d for measured and estimated values respectively), there is a greater fluctuation of the measured data around the net area line than the one associated to the residual strength parameter. This fluctuation, however, is limited to the interval [−10%, +10%] relative to the net area line for a wide range of remaining cross-sectional area values (from 57% to 100%) considered in the analysis.

The dependency of the deformation capacity of the damaged strands as function of the damage level and degree of asymmetry (*IA* values) are presented in Fig. 11e and f respectively. The net are line curve is included as a reference curve in Fig. 11e. In these both plots, it is observed that measured and estimated curves approach to a unique measured and estimated curve respectively, in which some consistent deviation is found for the measured 10.1 mm diameter strand curves. Considering the 1×7 stands geometry, both, measured and predicted data, decrease as the damage level and *IA* values increase, having the measured data a steeper decreasing rate reaching a minimum average value equal to 71% of the virgin measured value for a remaining cross-sectional area value of 57% of the virgin strands cross-sections and an *IA* value equal to 0.5. For the same aforementioned maximum damage level and *IA* values, the average estimated value is equal to 95% of the virgin one. The 1x19 damaged metallic strand, however, show a somewhat different dependency on *IA* values: measured and predicted data suggest that the minimum deformation capacity (76% and 96% of the virgin value for the measured and predicted data respectively) is reached for an *IA* value equal to 0.21 to then increase to percentages equal to 82 and 98 correspondingly for an *IA* value equal to 0.5. This difference in the response of the 1×7 and 1×19 damage strands is consistent with the fact that one of the variables that rules damaged strand response is the type of strand construction (number of wires, wires arrangement, helical parameters, wire diameters, etc.) as reported in the literature [7–15]. Based on this analysis, it seems that for the strands considered in this study, the dependency of the deformation capacity on strand diameter and strand material is weak, because the aforementioned progression curves tend to approach to a unique curve, except for the 10.1 diameter AL strand case that consistently has lower values as previously discussed. More analyses and data are needed, however, to better understand the effect of damage level and the degree of asymmetry of damage distribution on the deformation capacity of damaged strands due the difficulties encountered in some of the tests performed and the fact that *NLBM* does not incorporate the effect of contact and frictional forces among strand wires on strands failure.

A summary of the residual strength, deformation capacity, and elastic stiffness values given by the *NLBM* along with experimental data is presented in Table 3. Based upon the data listed in the aforementioned table, the major difference between measured and estimated values is related to the deformation capacity of damaged strands, especially for the 1×7 aluminium strands (diameters equal to 10.1 mm and 14.3 mm). In some of

Table 3
Summary of the residual strength, elastic stiffness and deformation capacity values of asymmetrically damaged strands.

Strand Diameter [mm]	Damage Level	Residual Strength (kN)		Elastic Stiffness (kN) × 10^3		Deformation Capacity	
		Measured	Estimated	Measured	Estimated	Measured	Estimated
9.5	Virgin	72.2–72.9	76.1	10.2–10.4	10.3	0.082	0.082
	1-D	62.6–63.1	64.6	8.65–9.07	8.89	0.076	0.08
	2-D	51–53.3	53.9	6.9	7.39	0.064	0.079
	3-D	38.8–42.8	43.9	6.2–6.3	6.04	0.06	0.078
10.1	Virgin	16.9	20	3.7	3.9	0.049	0.074
	1-D	14.1–14.4	16.8	2.8–3.05	3.36	0.04	0.072
	2-D	13.2–13.3	14.6	2.6–2.8	2.8	0.035	0.072
	3-D	10.7–10.9	11.4	2.0	2.24	0.03	0.07
12.7	Virgin	130.5–130.7	139.4	14.5–19.0	19.04	0.083	0.081
	1-D	109.3–111.9	118	13.8–15.4	16.0	0.076	0.08
	2-D	91.7–92.7	97.1	11.8	13.2	0.064	0.079
	3-D	62.8–70.4	78.4	9.02–9.2	10.8	0.06	0.077
14.3	Virgin	38.2–39.4	39.9	7.1–7.7	7.8	0.063	0.074
	1-D	33.1–34.9	34.1	5.85–6.8	6.69	0.056	0.072
	2-D	28.8–29.3	28.4	5.01–5.76	5.57	0.05	0.071
	3-D	23.7	22.7	4.3–4.37	4.46	0.048	0.069
19.9	Virgin	73.2–78.9	67.3	12.5–12.8	12.8	0.071	0.074
	2-D	69.4–70.4	60.5	10.6–11.3	11.75	0.064	0.072
	4-D	59.9–60.1	56.3	9.2–10.0	10.44	0.058	0.073
	6-D	52.2–54	46.3	8.1	9.08	0.054	0.071

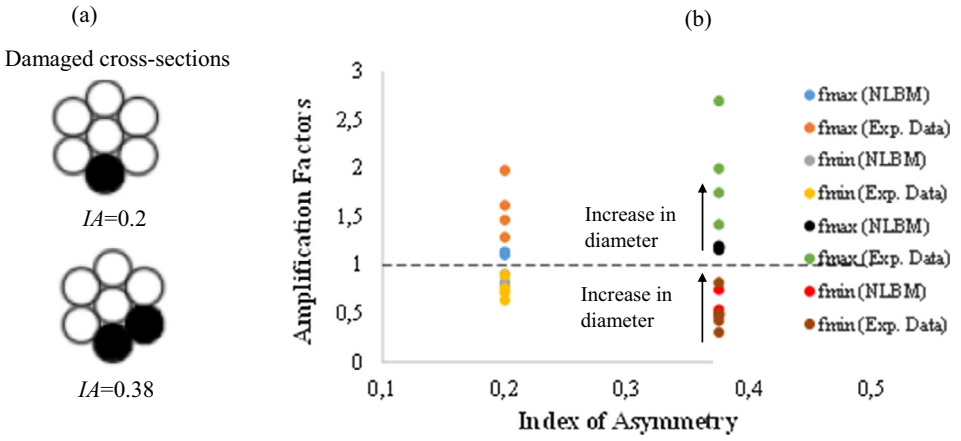

Fig. 12. (a) Damaged cross-sections and *IA* values; (b) diameter and *IA* effects on axial strain gradient throughout cross-section.

the tests performed, as the strands are asymmetrically damaged, unevenly strain/stress distributions are developed within strand cross-section as discussed previously in Figs. 7 and 10. For this type strain/stress distribution, the role of contact forces on the failure strain values is even more relevant especially for a soft material as aluminium, particularly for cross-sections with thin and few unbroken wires (1 × 7 cross-section) available to redistribute contact forces. Thus, this unevenly strain/stress distribution in strand terminations induces a premature failure of the strands. In fact, the measured virgin strength values obtained from capacity tensile tests are greater than the minimum breaking strength provided by the strands suppliers listed in Table 1, except for the case of the 10.1 mm diameter AL strand whose failure regions were consistently located near to one of the socket, reducing its virgin breaking strength value. The proposed *NLBM* does not consider contact forces effect on damaged strand response; hence, estimated values of the deformation capacity of damaged strands do not have a significant reduction as the damage level and index of asymmetry values increase (Table 3). This conclusion is consistent with one associated to the comparisons of deformation capacity values provided by the 3D FEM and *NLBM* discussed in Fig. 6d. As such, the most representative values of the measured deformation capacity are reported in Table 3 and rather than comparing absolute measured and estimated deformation capacity values, the analysis of the progression of the normalized quantities (with respect to the corresponding virgin values) relative to the remaining cross-sectional area and *IA* values is presented in Fig. 11e and f.

The values of the apparent modulus of elasticity obtained from the capacity tests on virgin ST and AL strands reported in [31], are used to calculate the value of the modular ratio between the steel and aluminium. In this way, the aluminium strands are transformed into equivalent steel strands whose diameter values depend upon the aforementioned modular ratio value. The values considered in this computations are: $E_{app\text{-}ST}$ and $E_{app\text{-}AL}$ equal to 153 GPa and 65 GPa, which are the apparent elastic moduli of steel and aluminium respectively. The aforementioned values compare well with the E_Q (modulus of elasticity for persistent design situations during service) value specified in [32] for steel spiral strand ropes (150 ± 10 GPa) and with the modulus of elasticity for 1 × 7 aluminium strands (59 GPa) listed in [33]. As such, the modular ratio value considered is 2.3 and the corresponding equivalent diameter values of steel strands are 7.0 mm and 9.8 mm for the 10.1 mm and 14.3 mm diameter aluminium strands respectively. Having all the tested specimens of the same material (steel in this case) and using the principle of strain equivalence (i.e., aluminium conductors and their equivalent steel strands develop the same axial strain field), the amplification factors are computed, f_{max} for the wires adjacent to damage and f_{min} for the wires opposite to damage, and their dependency on both diameter of equivalent strand and *IA* values are studied. Two damage distributions are considered for this purpose: one and two out of seven wires cut (colored black in Fig. 12a) whose *IA* values are 0.2 and 0.38 respectively. Based on the results presented in Fig. 12b and Table 4, for a fixed *IA* value, as the diameter value increases, both estimated (given by the *NLBM*) and measured f_{max} (values above horizontal dashed line at 1) and f_{min} (values below horizontal dashed line at 1) values increase as well. The rate of increase of both measured parameters is greater for the f_{max} parameter for *IA* equal to 0.2

Table 4
Measured and estimated amplification factors and estimated lateral deflection.

IA value	Strand diameter [mm]	f_{max} factor		f_{min} factor		f_{gsf} factor		Lateral deflection [mm]
		Measured	*NLBM*	Measured	*NLBM*	Measured	*NLBM*	*NLBM*
0.2	7.0	1.29	1.11	0.64	0.78	2.01	1.42	0.47*
	9.5	1.47	1.12	0.72	0.81	2.04	1.38	0.53
	9.8	1.62	1.13	0.76	0.83	2.13	1.36	0.17*
	12.7	1.98	1.14	0.90	0.91	2.20	1.25	0.32
0.38	7.0	1.42	1.16	0.31	0.48	4.58	2.42	1.2*
	9.5	1.75	1.18	0.43	0.5	4.06	2.36	1.39
	9.8	2.0	1.19	0.5	0.54	4.0	2.20	0.43*
	12.7	2.7	1.20	0.82	0.75	3.29	1.60	0.84

* () Values computed considering the aluminium strands.

and greater for f_{min} for *IA* equal to 0.38; thus the measured gradient in the strain field (parameter $f_{gsf} = f_{max}/f_{min}$) is greater for larger diameter values for *IA* equal to 0.2 (f_{gsf} value increases from 2.01 to 2.20) and gets smaller for larger diameter values for *IA* equal to 0.38 (f_{gsf} value decreases from 4.58 to 3.29). Contrary, for both *IA* values, the estimated gradient decreases as the strand diameter increases (f_{gsf} value decreases from 1.42 to 1.25 for $IA = 0.20$ and from 2.46 to 1.6 for $IA = 0.38$), because f_{max} is nearly constant and f_{min} gets larger as strand diameter increases (Table 4). Both estimated and measured strain field gradient (f_{gsf}) increase under the following conditions: for larger values of *IA* and fixed strand diameter values and if both *IA* and strand diameter values increase (f_{max} increases and f_{min} decreases). It is important to point out that measured f_{gsf} values are greater than the estimated ones within a range of 1.42–2.06, in which the difference between these values is mainly due to the f_{max} values. In fact, both estimated and measured f_{min} values compare quite well between each other (estimated values are bounded by measured ones @@(Fog. 12b)), but measured f_{max} values are greater than the estimated ones within a range of 16%–125%. It is believed that the aforementioned difference could be the result of that the localized inflicted damage perturbs the strain gauges measurements in the wires adjacent to it, which in fact are related to the amplification factor f_{max}. In addition, maximum lateral deflection values in the elastic range of the tested damaged strands given by the *NLBM* are listed in Table 4. For the case of one wire cut ($IA = 0.2$), lateral deflection values range from 1% to 5.5% of the diameter strand values. For the case of two wires cut ($IA = 0.38$), these values are in the range of [3%, 15%] relative to the diameter strand values. Although the damage level values considered exceed the 10% of the strand virgin cross-sections, established as a discard criterion for visible broken wires in [4,34], the estimated lateral deflections are relatively small suggesting that the original straight strand configurations are slightly perturbed by the loss of cross-sectional symmetry of the strands. These values are not measured during the experimental tests.

5. Conclusions

In this paper, a robust and computational efficiency numerical model is proposed to estimate the static response of multilayered strands asymmetrically damaged on their surfaces. The proposed model relies on the assumption that a strand asymmetrically damaged on its surface behaves as a 1D nonlinear beam under uncoupled biaxial bending and axial load along with the fact that strand wires are mainly in radial contact. The proposed model is validated by comparisons with the results provided by 3D FE simulations and experimental data obtained from an experimental program performed in this study. Two types of metallic strand construction, made of steel and aluminium, are considered for the numerical validation and experimental testing: 1×7 and 1×19, with diameter values that range from 3.5 mm to 22.2 mm and a wide range of damage level (from 5% to 43% of the strand cross-section damaged) and different degree of asymmetry in damage distribution (captured by the index of asymmetry *IA* values).

Based on the comparisons performed, the proposed model captures the dependency of the damaged strand response on type of the strand construction and damage level, degree of asymmetry, and strand diameter values. The analyses made reveal that the response (residual strength and stiffness) of metallic strands asymmetrically damaged on their surfaces is mainly governed by the net area effect in which the loss of symmetry of the cross-section slightly perturbs the straight strand configuration inducing some small bending deformation that reduces the deformation capacity of the strand relative to the virgin case (up to 8%), based on the results of the numerical simulations. The bending deformation gives rise to a gradient in the axial strain field within strand cross-section in which greater and smaller strains are developed in wires adjacent and opposite to damage respectively. The estimated ratio between the maximum and minimum strain developed in the elastic regime ranges from 1.1 to 2.5, for all the cases studied. In addition, waviness of the damaged strand is also induced in which most of the values computed in the elastic regime are in the range of 1%–5% of the corresponding strand diameter value.

The proposed model seems to be a promising computational tool to provide some information on the integrity of damaged strand based on some discard criteria specifically applied to strands. In particular, this model can be used to assess the potential damage distribution within strand cross-section by a trial and error procedure based upon strand distortion (waviness) measurements obtained during regular inspections; it can reduce the need of conducting expensive and time-consuming tests on damaged strands to determine if they are replaced or not based on some discard criteria; it can be combined with a (magnetic) non-destructive quantification of loss of metallic cross-sectional area (*LMA*) for assessment of strand condition and correlate *LMA*, loss of strand strength (*LSS*), and strand distortion; and it can evaluate the bending effect on damaged strand modeling. If bending curvature is big enough, unbroken wires slip between each other inducing a nonlinear bending response of the damaged strand [23–25].

Regardless of the good performance of the proposed model described in this paper, additional comparisons with numerical models based upon well-accepted technique (e.g., 3D FEM) and experimental data that consider other strand materials and strand constructions are needed to established the range of its applicability to estimate the static response of a multilayered strand asymmetrically damaged on its surface. Strand wires are treated as tensile elements in the proposed model, neglecting its transverse deformation. Due to the complex interaction between strand wires owing to their curved configuration along strands length, a more general model that treats each wire as a rod element to include transverse deformation and frictional, local bending, and contact effects needs to be explored. Despite these limitations, and based on the preliminary results presented in this paper and the low computational cost relative to the 3D FE models, the proposed model seems to be a promising computational tool to estimate the static response of a of a multilayered strand asymmetrically damaged on its surface.

Conflicts of interest statement

The authors of this manuscript confirm that there are no known conflicts of interest associated with this publication.

Acknowledgements

This work was supported by Fondecyt (Chile) Grant N° 1150409. The authors gratefully acknowledge this funding. The help of Mr. Pedro Soto and Victor Gonzalez during the experimental program is also deeply appreciated.

Appendix

A. Numerical algorithm to estimate asymmetrically damaged strand response

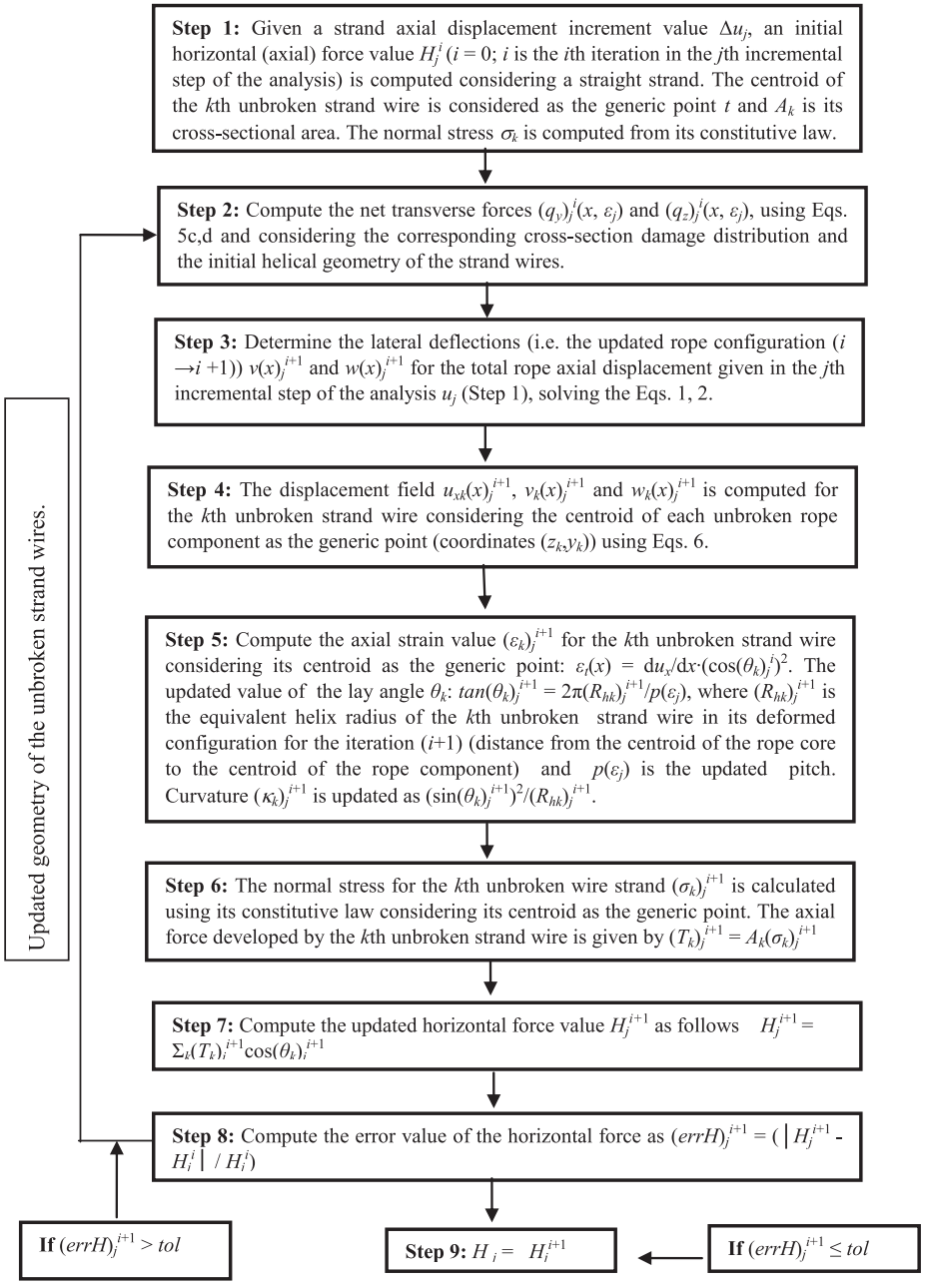

In the above algorithm, the variable *tol* is a prescribed tolerance (5E-4 used in this study) set to establish the convergence of the algorithm. In addition, the initial value of the horizontal axial force H_j^0 (Step 1) can be estimated as

$$H_j^0 = \sum_k A_k \sigma_k \left(\frac{u_j}{L_0} \left[\cos(\theta_0)_k \right]^2 \right) \cos(\theta_0)_k \quad (A.1)$$

where u_j is the total strand axial displacement in the jth incremental step of the analysis; L_0 and θ_0 are the initial strand

length and lay angle of the kth unbroken strand wire respectively.

References

[1] A. Cardou, C. Jolicoeur, Mechanical models of helical strands, Appl. Mech. Rev. 50 (1) (1997) 1–14.
[2] W.S. Utting, N. Jones, N, A survey literature on the behaviour of wire ropes, Wire Ind. 51 (1984) 623–629.
[3] C.R. Chaplin, The fatigue and degradation mechanisms of hoisting ropes, Hoist and Haul Conference, Perth, Australia, 2005, pp. 359–366.
[4] M. van Zyl, Discard criteria for mine winder ropes, Report GAP502, Safety in Mines, Res. Advisory Committee (2000).
[5] Wire Rope Users Manual, fourth edition, Wire Rope Technical Board, Virginia, 2005.
[6] ISO 4309 Cranes-Wire ropes-Care and maintenance, inspection and discard, 2010.
[7] C.R. Chaplin, N.N. Tantrum, The influence of wire break distribution on strengthOrganisation Internationale pour l'Etude de l'Endurance des Cables (OIPEEC), Round table conference, Glasgow, Scotland, 1985.
[8] W. Cholewa, Wire fracture and weakening of wire rope, Wire rope discard criteria: round table conference. Swiss Federal Institute of Technology (ETH), Institute of Lightweight Structures and Ropeways, Zurich, Switzerland, 1989.
[9] J.J. Evans, I.M.L. Ridge, C.R. Chaplin, Wire failures in ropes and their influence on local wire strain behavior in tension–tension fatigue, J. Strain Anal. 36 (2001) 231–244.
[10] C. MacDougall, F. Bartlett, Mechanical model for unbonded seven-wire tendon with single broken wire, J. Eng. Mech. 132 (12) (2006) 1345–1353.
[11] H. Mouradi, A. El Barkany, A. El Biyaali, Steel wire ropes failure analysis: experimental study, Eng. Fail. Anal. 91 (2018) 234–242.
[12] J. Lanteigne, Theoretical estimation of the response of helically armoured cables of tension, torsion, and bending, J. Appl. Mech. 52 (1985) 423–432.
[13] M. Raoof, Wire recovery length in a helical strand under axial-fatigue loading, Int. J. Fatigue 13 (2) (1991) 127–132.
[14] C. MacDougall, F. Bartlett, Mechanical model for unbonded seven-wire tendon with symmetric wire breaks, J. Eng. Mech. 131 (12) (2005) 1239–1247.
[15] M. Lepidi, V. Gattulli, F. Vestroni, Static and dynamic response of elastic suspended cables with damage, Int. J. Solids Struct. 44 (2007) 8194–8212.
[16] J.F. Beltran, E. De Vico, Assessment of static rope behavior with asymmetric damage distribution, Eng Struct. 86 (2015) 84–98.
[17] J.F. Beltran, D. Vargas, Effect of broken rope components distribution throughout rope cross-section on polyester rope response: numerical approach, Int. J. Mech. Sci. 64 (2012) 32–46.
[18] J.F. Beltran, N. Ramirez, E. Williamson, Simplified analysis of the influence of strain localization and asymmetric damage distribution on static damaged polyester rope behavior, Ocean Eng. 145 (2017) 237–249.
[19] G.A. Costello, Theory of Wire Rope, second ed., Springer-Verlag, New York, 1997.
[20] R. LeClair, Axial response pf multilayered strands with compliant layers, J. Eng. Mech. 117 (1991) 2884–2903.
[21] W.G. Jiang, M.S. Yao, J.M. Walton, A concise finite element model for simple straight wire rope strand, Int. J. Mech. Sci. 41 (1999) 143–161.
[22] R. Judge, Z. Yang, S.W. Jones, G. Beattie, Full 3D finite element modelling of spiral strand cables, Constr. Build. Mater. 35 (2012) 452–459.
[23] Y. Yu, Z. Chen, H. Liu, X. Wang, finite element study of behavior and interface force conditions of seven-wire strand under axial and lateral loading, Constr. Build. Mater. 66 (2014) 10–18.
[24] S.-Y. Kim, P.-S. Lee, Modeling of helically stranded cables using multiple beam finite elements and its application to torque balanced design, Constr. Build. Mater. 151 (2017) 591–606.
[25] F. Foti, L. Martinelli, An analytical approach to model the hysteresis bending behavior of spiral strands, Appl. Math. Model. 40 (2016) 6451–6467.
[26] S. Lalonde, R. Guilbault, F. Legeron, Modeling multilayered wire strands, a strategy based on 3D finite element beam-to-beam contact-Part I: model formulation and validation, Int. J. Mech. Sci. 126 (2017) 281–296.
[27] I. Silva, Análisis de cables superficialmente dañados en forma asimétrica con geometría multicapa: Modelos numéricos en elementos finitos, University of Chile, Chile (Spanish), Thesis Civil Engineering, 2017.
[28] C. MacDougall, Behaviour of monostrands tendons with broken wires PhD dissertation, The University of Western Ontario, Ontario, Canada, 2001.
[29] D. Li, A. Miyase, J.G. Williams, S.S. Wang, Damage tolerance of synthetic- fiber mooring ropes: small-scale experiments and analytical evaluation of damaged subropes and elements Technical report CEAC-TR-03-0101, University of Houston, 2002.
[30] G. Rebel, M. Borello, H.D. Chandler, On the torsional behaviour of triangular-strand of hoisting rope, J. S Afr I Min. Metall (1996) 279–287. Nov.
[31] F. Nuñez, Influencia en la distribución del daño en curvas de capacidad de cables: Análisis Experiemntal, University of Chile, Chile (Spanish), Thesis Civil Engineering, 2017.
[32] Eurocode 3-Design of steel structures-Part 1-11: Design of structures with tension components, 2006.
[33] Trefinasa, Overhead Conductors Catalogue, 2016.
[34] Guidance on the selection installation, maintenance, and use of steel wire ropes in vertical mine shafts first edition, 2004, Deep Mined Coal Industry Advisory Committee Norwich.